Journal of Solid State Chemistry **151,** 272–280 (2000)
doi:10.1006/jssc.2000.8653, available online at http://www.idealibrary.com on IDEAL®

Effect of the Mg : Al Ratio on Borate (or Silicate)/Nitrate Exchange in Hydrotalcite

M. del Arco,* S. Gutiérrez,* C. Martín,* V. Rives,*,[1] and J. Rocha†

** Departamento de Química Inorgánica, Universidad de Salamanca, Salamanca, Spain; and †Departamento de Química, Universidade de Aveiro, Aveiro, Portugal*

Received October 21, 1999; in revised form January 11, 2000; accepted February 18, 2000

Layered double hydroxides (LDHs) have been prepared with interlayer nitrate and with different Mg : Al ratios. Solids with low Mg : Al ratios show larger basal spacings than those with larger Mg : Al ratios, consistent with tilting of the nitrate ions, respectively. Nitrate/tetraborate and nitrate/silicate anionic exchange has been achieved only for those samples with "tilted" nitrate. The precise nature of the interlayer species in the exchanged samples has been concluded from MAS–NMR results. The layered structure of the exchanged samples collapses at temperatures higher than those for the nitrate-containing precursors. © 2000 Academic Press

INTRODUCTION

Layered double hydroxides (LDHs), also known as "anionic clays," have received much interest in the past decade because of their potential applications in different fields (1, 2). Structurally, they are formally derived from brucite, $Mg(OH)_2$, by a partial Mg^{2+}/Al^{3+} substitution in the octahedral holes, the positive charge being balanced by interlayer anions, usually carbonate, although many other anions are known in minerals and synthesized LDHs. These materials constitute the only family of layered solids known with a permanent positive charge in the layers. The mineral hydrotalcite displays this type of structure and has the formula $Mg_6Al_2(OH)_{16}CO_3 \cdot 4H_2O$, although in order to show its relationship with the structure of brucite, it is often formulated as $[Mg_{0.75}Al_{0.25}(OH)_2](CO_3)_{0.125} \cdot 0.5H_2O$.

The main interest of LDHs is their ability to exchange interlayer anions, thus presenting an enormous potentiality for preparing materials with a wide range of chemical compositions (3). However, carbonate is strongly held and, hence, alternative methods have been developed to introduce other anions, for example direct synthesis in the presence of the desired anion and reconstruction of the layered structure from a partially decomposed hydrotalcite (4). Unfortunately, the latter usually yields poorly crystallised materials and, thus, anionic exchange or direct synthesis are preferred (5–9). However, when the size of the entering anion is much larger than that of the exiting anion the exchange is difficult and alternative routes must be developed. Swelling of the layers with a polyalcohol has been used in certain cases (6, 9).

Although much interest has been devoted to the synthesis of LDHs with metal-containing anions (10), very little work has been carried out with inorganic nonmetal anions. However, it is obvious that introduction of anions such as silicate, phosphate, or borate may deeply modify the surface acid/base properties of these solids. Chen and Lin (11) did not succeed in obtaining a LDH-borate either by direct synthesis in the presence of borate (an amorphous solid was obtained) or by nitrate exchange. A LDH-$B_4O_5(OH)_4$ material was obtained by preswelling the layers with adipate ($C_6H_8O_4^{2-}$). Li *et al.* (12) introduced tetraborate in LDH by exchanging and hydrothermally treating with $Na_2B_4O_5(OH)_4 \cdot 8H_2O$ the suspension obtained by precipitating a mixture of Mg and Al nitrates. However, if the basic nitrate is dried, a partial exchange occurs only after a severe hydrothermal treatment. Battacharyya and Hall (13) have reported the preparation of a LDH-triborate by direct synthesis with boric acid.

Anionic exchange from LDH-Cl has been successfully used by Schutz and Biloen (14) to prepare LDH-silicate materials. Powder X-ray diffraction and ^{27}Al and ^{29}Si MAS NMR suggested the presence of interlayer $[HSi_2O_5]_n^{n-}$ polymers. Fyfe *et al.* (15) have reported a partial $Cl^-/Si_8O_{20}^{8-}$ exchange in LDH-Cl, but only when the molar Mg : Al ratio is equal or lower than 3 (this ratio is related to the positive charge in the layers and, thus, to the electrostatic forces between the layers and the interlayer anions). Carbonate contamination prevents a complete exchange.

Yun *et al.* (16) used tetraethylorthosilicate to intercalate silicate in LDHs starting from synthetic meixnerite, the

[1] To whom correspondence should be addressed. E-mail: vrives@gugu.usal.es.

0022-4596/00 $35.00
Copyright © 2000 by Academic Press
All rights of reproduction in any form reserved.

Mg,Al LDH with interlayer hydroxyl groups. According to these authors, silicate anions are formed by hydrolysis and condensation of silanol groups. As the amount of Al in the layers is increased, exchange of hydroxyde for silicate becomes more difficult, due to the enhanced electrostatic interaction between the positive layers and the interlayer hydroxyl groups.

In the present paper, we report on the incorporation of tetraborate and silicate in Mg, Al LDHs by anion exchange from a LDH-nitrate precursor in order to study the effect of the Mg : Al ratio on the exchange process. Evolution of the chemical species formed upon calcination of the borate and silicate LDHs at increasing temperatures is also studied.

EXPERIMENTAL

Synthesis of the Samples

Synthesis of the LDH-nitrate precursor. All solutions were prepared using water previously decarbonated by boiling and bubbling N_2. A solution prepared by dissolving 64.1 g $Mg(NO_3)_2 \cdot 6H_2O$ and $Al(NO_3)_3 \cdot 9H_2O$ (the amount required for Mg : Al ratios of 2 or 4) in 125 ml H_2O was added dropwise to 250 ml of water, to which a solution (NaOH 2M, $NaNO_3$ 1M) was being simultaneously added to maintain pH 10. The synthesis was carried out at 40°C while the suspension was being stirred magnetically. The precipitates were washed with water to remove "free" (i.e., not interlayered) nitrates. A small portion was withdrawn for analysis and characterization and the suspension was used to prepare the borate and silicate samples.

Synthesis of LDH-borate. A solution prepared by dissolving 5.38 g $(NH_4)_2B_4O_7 \cdot 4H_2O$ (20.4 mmol) in 50 ml H_2O was added dropwise to 150 ml of the suspension (ca. 3 g solid/100 ml suspension) of the 2N nitrate precursor (exchange capacity 380 meq/100 g); the final pH was 9.47. The suspension was magnetically stirred and heated at 90°C for 10 h (a reflux refrigerant was used to avoid evaporation of the solvent), while N_2 was continuously bubbled. The precipitate was filtered, washed with water and dried at room temperature.

Synthesis of LDH-silicate. A solution of sodium silicate (SiO_2–NaOH–H_2O) prepared by dissolving 1.62 g SiO_2 (27 mmol) and 0.52 g NaOH (13 mmol) in 270 ml H_2O was added to 25 ml of the hydrotalcite suspension (ca. 11 g/100 ml suspension). The suspension was magnetically stirred and heated at 85°C for 4 h while N_2 was continuously bubbled. The precipitate was filtered, washed, and dried at room temperature.

The samples are named XY, where $X = 2$ or 4 (nominal Mg : Al ratio), and Y = N, B, Si, depending on the interlayer anion.

Techniques

Elemental chemical analyses for Mg and Al were carried out in Servicio General de Análisis Químico (University of Salamanca, Spain) by atomic absorption in a Mark 2 ELL-240 instrument after dissolving the samples in nitric acid.

Powder X-ray diffraction diagrams (PXRD) were collected on a Siemens D-500 using Cu$K\alpha$ radiation (λ = 1.54050 Å) and quartz as an external standard.

Differential thermal analysis (DTA) and thermogravimetric analyses (TGA) were measured on DTA7 and TGA7 instruments, respectively, from Perkin–Elmer. The analyses were carried out in flowing (30 ml/min) oxygen from L'Air Liquide (Spain).

Fourier-transform infrared spectra (FT–IR) were collected in a Perkin–Elmer FT1730 instrument using the KBr pellet technique; 100 scans were averaged to improve the signal-to-noise ratio at nominal resolution of 4 cm^{-1}.

^{11}B MAS NMR spectra were recorded at 128.4 MHz on a Bruker MSL 400P spectrometer using short, 0.6-μs (equivalent to 15°) radio-frequency pulses, 2-s recycle delay, and very fast (30 kHz) spinning rate. Chemical shifts are quoted in ppm from $BF_3 \cdot O(C_2H_5)_2$. ^{27}Al MAS NMR spectra were recorded at 104.3 MHz using short, 0.6-μs (equivalent to 10°) radio-frequency pulses, 1-s recycle delay, and 30-kHz spinning rates. Chemical shifts are quoted in ppm from $Al(H_2O)_6^{3+}$. ^{29}Si MAS NMR spectra were recorded at 79.5 MHz using 3-μs (equivalent to 50°) radio-frequency pulses, 60-s recycle delay, and 5-kHz spinning rate. ^{1}H–^{29}Si CP/MAS NMR spectra were recorded at 79.5 MHz using 5-μs 90° pulses, a contact time of 2 ms, 5-s recycle delay, and 5-kHz spinning rate. Chemical shifts are quoted in ppm from TMS.

RESULTS AND DISCUSSION

Nitrate and Exchanged Samples

Chemical analyses (Mg and Al) for samples 2N, 4N, 2B, and 2Si are given in Table 1. For samples 2N and 4N the analyses for N were in agreement with the Al conent (i.e., a N : Al molar ratio close to one), while C content was close to zero. PXRD (data not shown) indicate no change in the basal spacing for samples 4B and 4Si, thus indicating that exchange did not take place; so, these samples will not be discussed here. The chemical formulae given in Table 1 have been derived assuming (data shown below) that nitrate or tetraborate is the only interlayer anion in the corresponding sample. On the other hand, no definitive formula for the interlayer silicate in sample 2Si could be unambiguously concluded from the studies here reported, and so no formula is given.

The Mg : Al ratios of the parent solutions and the samples obtained are very similar. Only for sample 2Si a small (5%) deviation is observed. It has been reported (9, 17–20) that

TABLE 1
Chemical Composition (Metals) and Formulas of the Samples Studied

Sample	%Al*	%Mg*	Mg:Al**	Formula
2N	10.1	18.5	2.0	$[Mg_{0.67}Al_{0.33}(OH)_2]\ (NO_3)_{0.33}\cdot 0.4\ H_2O$
4N	3.8	13.5	4.0	$[Mg_{0.8}Al_{0.2}(OH)_2]\ (NO_3)_{0.2}\cdot 0.48\ H_2O$
2B	9.3	17.0	2.0	$[Mg_{0.67}Al_{0.33}(OH)_2]\ [(B_4O_5(OH)_4]_{0.16}\cdot 0.61\ H_2O$
2Si***	7.9	14.8	2.1	see text

* Weight percentage.
** Atomic ratio.
*** 7% Si.

the exchange process leads to changes in the layers M^{2+}/M^{3+} ratio of the parent solid and the material obtained after exchange. This is probably due to a partial dissolution of the layers when the exchange (e.g., polyoxometalates) is carried out at neutral or acidic pH. Such conditions are also used to remove interlayer organic anions which are neutralized in these conditions and are easily removed (exchanged) from the interlayer space. In the present case, because the exchange has been carried out at pH 9–10 such a dissolution should be hindered.

The PXRD patterns for all four samples are shown in Fig. 1 and correspond to well-crystallized layered materials. The peaks recorded are attributed to crystalline planes of a hydrotalcite structure (3*R* symmetry) (21–23) (Table 2). The *c* parameter has been calculated from the first three harmonics, ascribed, respectively, to planes (003), (006), and (009). The parameter *a* has been calculated from the position of the first peak in the doublet close to $2\theta = 60^\circ$ given by planes (110) (2) according to

$$c = d_{003} + 2d_{006} + 3d_{009}$$

$$a = 2d_{110}.$$

The pattern of sample 4N shows, in addition to strong peaks due to the hydrotalcite structure, weak reflections at 4.7, 1.8, and 1.57 Å, attributable to small amounts of $Mg(OH)_2$.

Parameter *a* for samples 2N and 4N increases as expected with increasing Mg:Al because it is directly related to the distance between two neighboring octahedra in the brucite-like layers. This distance decreases with increasing Al^{3+} content of the layers because this ion is smaller than Mg^{2+} (ionic radii 0.68 and 0.86 Å, respectively) (24).

The d_{003} spacing corresponds to the distance, along the *z* axis, between the centers of two consecutive brucite-like layers. The gallery height can be calculated from d_{003}, after

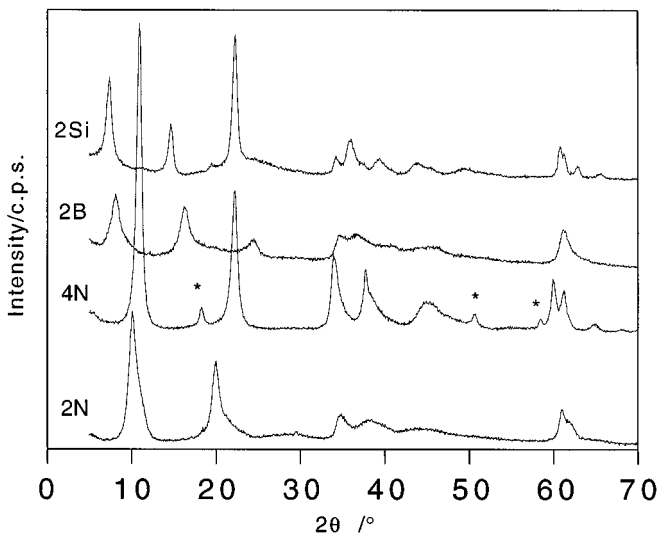

FIG. 1. Powder X-ray diffraction patterns of precursors 2N and 4N and samples 2B and 2Si. The asterisks depict the maxima due to $Mg(OH)_2$.

TABLE 2
Attribution of PXRD Peaks and Lattice Parameters for Samples 2N, 4N, 2B, and 2Si*

2N		4N		2B		2Si		(*hkl*)
d_{exp}	d_{cal}	d_{exp}	d_{cal}	d_{exp}	d_{cal}	d_{exp}	d_{cal}	
8.75	8.75	8.08	8.08	10.79	10.79	11.86	11.86	(003)
4.42	4.38	4.03	4.04	5.39	5.39	6.02	5.93	(006)
				3.62	3.60	3.97	3.95	(009)
2.58	2.58	2.62	2.61	2.59	2.59	2.61	2.61	(012)
2.35	2.35	2.37	2.34	2.45	2.43	2.48	2.47	(015)
2.05	2.05	2.00	2.00	2.00	2.19	2.28	2.27	(018)
						2.06	2.04	(0,1,11)
						1.84	1.89	(1,0,13)
1.52	1.52	1.54	1.54	1.51	1.51	1.52	1.52	(110)
1.50	1.51	1.51	1.51			1.51	1.51	(113)
						1.48	1.47	(116)
c 26.39		24.21		32.43		35.81		
a 3.04		3.08		3.02		3.04		

* All values in Å.

subtracting the width of the brucite layer, 4.8 Å (6). Samples 2N and 4N have different d_{003} spacings (8.8 and 8.0 Å, respectively). Thus, the gallery height for sample 4N corresponds to ca. 3.2 Å, fairly close to the diameter of an oxide anion (24). This result suggests that, as in Mg,Al–CO_3 hydrotalcites, the interlayer nitrate is in a "flat" position with the molecular plane parallel to the layers. In contrast, the width for sample 2N (4 Å) suggests that the nitrate anion is in a "tilted" position.

These results are similar to others previously reported for nitrate and carbonate-containing hydrotalcites (25, 26). When the Mg : Al ratio decreases, the net positive charge of the layers increases and a larger concentration of interlayer anions is required. While divalent carbonate may lay in a flat position, for monovalent nitrate there is not enough room in the interlayer space to accommodate the larger number of nitrate anions required for charge balancing and, thus, these ions become tilted.

The PXRD patterns of samples 2B and 2Si do not show any diffraction peaks due to nitrate-containing hydrotalcites indicating complete exchange; no exchange was achieved from sample 4N, despite using the very same experimental procedure. The interlayer spacings measured were 12.0 and 10.8 Å, respectively, for samples 2Si and 2B.

Cheng and Lin (11) claimed that borate exchange only proceeds if the layers are previously swelled with a bulk organic anion. Li *et al.* (12), however, proposed that exchange only takes place if the nitrate-containing precursor is held in suspension and is not completely dried before exchanging it with borate. Our results indicate a third possibility: first, exchange was achieved for precursor 2N without using any preswelling bulk organic anion. Second, the nitrate precursor was maintained in suspension for precursors 2N and 4N, but borate exchange was achieved only for the former. The experimental conditions and exchange ability were the same for the silicate samples. We conclude that the exchange ability is determined by the orientation of the nitrate anion in the interlayer space: when this ion is tilted the LDH structure is more expanded than when it is flat-oriented, thus favoring exchange even if a bulk anion is absent. However, when nitrate takes a flat orientation, the interlayer space is not large enough to allow an easy exchange. Our synthesis method provides, thus, an alternative, easier route to prepare borate-exchanged hydrotalcites.

The nature of the interlayer borate species cannot be concluded from the interlayer spacing values only, as close values have been ascribed in the literature to different species; so, Battacharyya and Hall (13) have ascribed the value of 10.8 Å to triborate species in an upward orientation (C_2 axis perpendicular to the layers) while the close value of 11.0 Å has been ascribed by Li *et al.* (12) to tetraborate species in their most stable orientation, as concluded from energy minimisation and geometry optimisation studies.

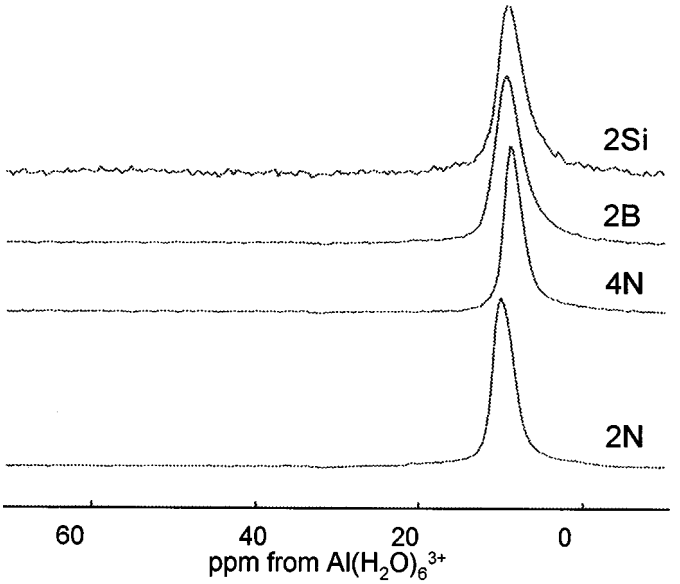

FIG. 2. ^{27}Al MAS NMR spectra of precursors 2N and 4N and samples 2B and 2Si.

Although both trigonal and tetrahedral local geometries exist in triborate and tetraborate, the trigonal:tetrahedral ratio is 2 : 1 in the former and 2 : 2 in the latter. As we shall see, ^{11}B MAS NMR spectroscopy helps in elucidating the nature of the interlayer borate anion in our material.

The ^{27}Al MAS NMR spectra of all four samples studied (Fig. 2) contain a single resonance centered at 9–10 ppm indicating the presence of six-coordinated aluminum. Close inspection reveals that the peak maximum shifts slightly from ca. 10.2 (sample 2N) to 9.1 ppm (2Si). The full-width-at-half-maximum (FWHM) of the resonances are ca. 310 (2N), 265 (4N), and 390 Hz (2B and 2Si). A larger FWHM may be due to an increasing quadrupole coupling constant brought about by a slightly stronger distortion of the local ^{27}Al environment. This is supported by the fact that the peak maximum shifts to lower frequency as the resonance gets broader. Indeed, it is well known that a larger quadrupole coupling constant results in both a broadening of the spectral lines and a larger quadrupole-induced shift to lower frequency (27). In addition, the lines may (among other reasons) be broadened by a dispersion of chemical shifts and quadrupole parameters arising from the presence in the sample of a range of slightly different ^{27}Al local environments.

The ^{29}Si MAS NMR spectrum of sample 2Si (Fig. 3) displays resonances at ca. -92, -99, and -110 ppm, which are assigned to $Si(OSi)_n(OH)_{4-n}$ or, in short, Q^n environments with $n = 2$, 3, and 4, respectively. This assignment is supported by the ^{29}Si CP/MAS NMR spectrum (Fig. 3) which exhibits only the peaks given by sites Q^2 and Q^3. It is

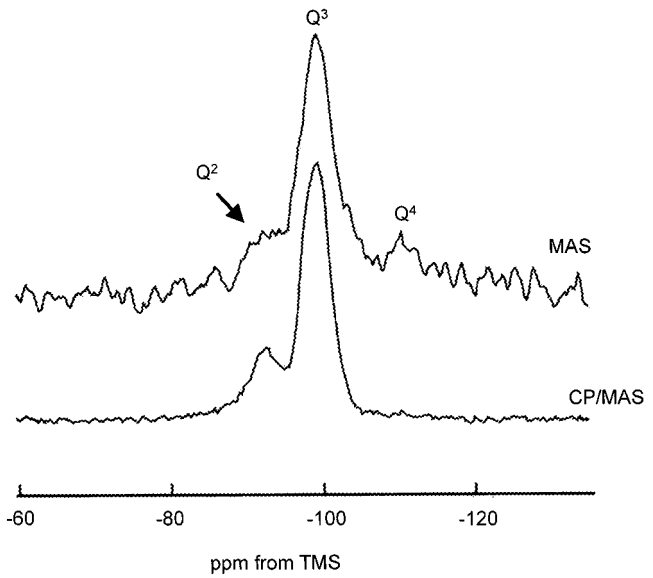

FIG. 3. ^{29}Si MAS and CP/MAS NMR spectra of sample 2Si.

well known that application of the CP technique leads to a strong and selective enhancement of these signals, with a characteristic dependence of the relative intensities on the chosen cross-polarization contact time, τ (27). At short τ (such as the 2 ms used to record the spectrum in Fig. 3), those silicons having the shortest Si–H distance, that is, the (Q^2, Q^3) silicons bearing OH groups, are most effectively cross-polarized and show the highest intensity. With increasing τ, silicons with larger Si–H distances (Si atoms in Q^4 units) give rise to increasing intensity of the signal at -110 ppm and dominate the spectrum at long τ (25–30 ms). The -92 and -99 ppm peaks may also have a contribution from Si local environments where silanols are replaced by OAl groups. The relative $Q^2 : Q^3 : Q^4$ populations (estimated via spectra deconvolution) are ca. 0.26 : 0.64 : 0.08.

The ^{11}B MAS NMR spectrum of sample 2B (Fig. 4) is characteristic of materials containing tetrahedral and trigonal boron (28). This spectrum has been simulated (taking into consideration both the central and the satellite transitions) and the quadrupole parameters, isotropic chemical shift, δ, quadrupole coupling constant, C_Q, and the asymmetry parameter, η, extracted: tetrahedral boron $\delta = 3.8$ ppm, $C_Q = 0.98$ MHz, $\eta = 0.93$; trigonal boron $\delta = 21.1$ ppm, $C_Q = 2.7$ MHz, $\eta = 0.01$. Since the relative populations of the two sites are in a ca. 1 : 1 ratio ^{11}B MAS NMR indicates the presence of tetraborate (and not triborate) species in the interlayer space.

The PXRD pattern (Fig. 1) of sample 2Si is similar to that reported by other authors (14–16). Although previous studies by Schutz and Biloen (14) and Yun *et al.* (16) reported the presence of some nonexchanged material, a single series of harmonics is recorded for sample 2Si indicating the presence of a single hydrotalcite-like material. Although the peaks recorded can be ascribed to the hydrotalcite structure (Table 2) their relative intensities (particularly the intensity of the $2\theta = 22^\circ$ reflection) do not coincide with the intensities observed with a Mg,Al–NO_3 sample. This may be due to the different electron density in the interlayer anions (29). Alternatively, the $2\theta = 22^\circ$ peak could be ascribed to the formation of cristobalite (JCPDS (30) file 11-0695). However, this seems unlikely because upon calcination at 250°C (see below) it disappears. In addition, the background intensity in the 20–25° 2θ range suggests the presence of some amorphous silica, as already reported in other studies (14, 16).

The FT–IR spectra of samples 2N and 4N (Fig. 5) are very similar. The differences which might be expected in the low-wavenumber region (under 1000 cm^{-1}) due to the different orientation of the nitrate anion in these samples are mostly obscured by the intense lattice bands involving Mg, Al, and OH ions. The weak band at ca. 1630 cm^{-1} is due to the deformation mode of the interlayer water molecules, while the intense band at 1380 cm^{-1} is ascribed to mode v_3 (antisymmetric stretching) of the nitrate anions (31), and the extremely weak peak close to 830 cm^{-1} is due to mode v_2 (out-of-plane bending). A broad, intense, band observed in the 4000–3000 cm^{-1} range is due to the OH stretching mode and is broadened due to the wide variety of hydrogen bonding with interlayer water molecules and interlayer anions. It should be noted that for sample 4N a shoulder is also recorded around 3000 cm^{-1}. A broad shoulder in this position has been previously reported (25, 32) and it has

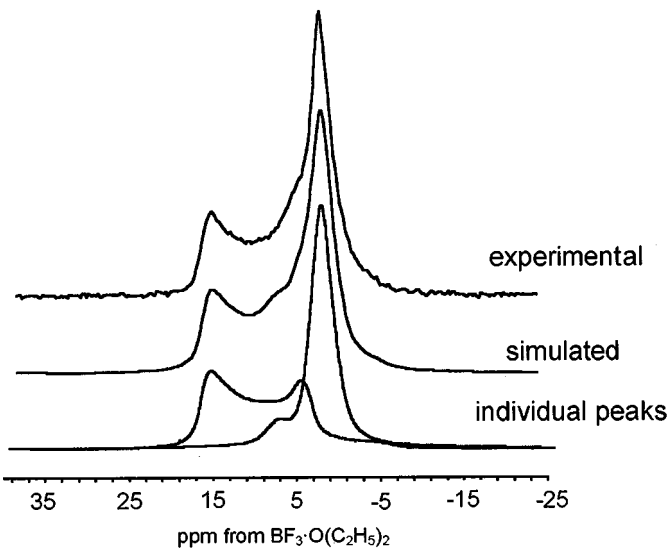

FIG. 4. Experimental and simulated ^{11}B MAS NMR spectra of sample 2B. The individual peaks used in the simulation are also shown.

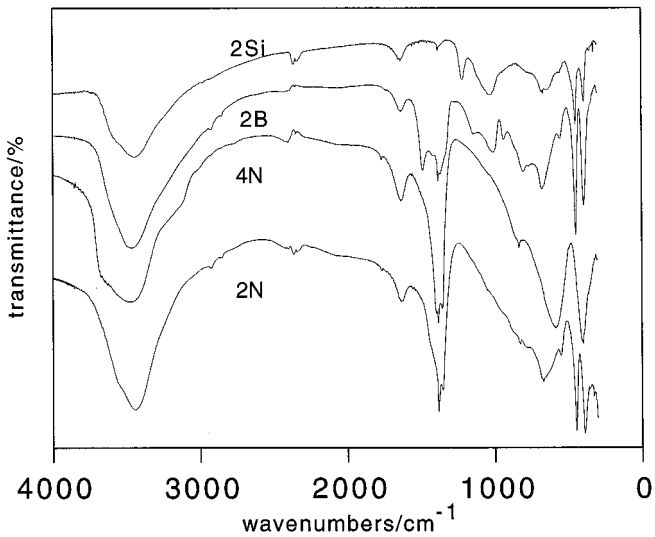

FIG. 5. FT–IR spectra of precursors 2N and 4N and samples 2B and 2Si.

been ascribed to the stretching mode of OH groups hydrogen-bonded to interlayer carbonate anions. It is possible that similar hydrogen bonding exists in this sample where (as carbonate) the nitrate anions are in a flat position.

In addition to the expected bands due to the hydrotalcite network, the FT–IR spectrum of sample 2B shows bands attributed to tetraborate confirming the results given above obtained by ^{11}B MAS NMR. Bands due to mode v_3 of trigonal borate and in-plane angular deformation of B–OH bonds are recorded between 1480 and 1300 cm^{-1}. Bands at 1146 and 1009 cm^{-1} are due to the same modes of tetrahedral borate, while bands due to the trigonal borate modes v_1 and v_2 are recorded at 939 and 805 cm^{-1}, respectively. The small differences between the positions of these bands for bulk tetraborate and for intercalated borate have been previously attributed by Li *et al.* (12) to changes in the B–O distances: elongation in the tetrahedral units and shortening in the trigonal units.

Finally, for sample 2Si a broad, very intense, band characteristic of layered silicates (33) is recorded at 1024 cm^{-1} together with a slightly weaker band at 1217 cm^{-1} due to the Si–O–Si units, the position of which has been related with the Si–O–Si angle (14). The bands between 1200 and 950 cm^{-1} have been ascribed to silicates in different states of polymerization (34). Other bands coincide with those for the hydrotalcite structure.

Calcined Samples

Preliminary results on the thermal stability of the nitrate and of the exchanged samples are here included. The aim is to identify the species existing after calcination at increasing temperatures, as the solids have been used in different catalytic reactions (35). In addition, thermogravimetric results have been used to calculate the number of water molecules in the interlayer space. The samples are named as XY–T, where X and Y have the same meaning as the original samples, and T stands for the calcination temperature in °C; calcination was carried out for 3 h in an open-air furnace.

The DTA and TG curves for all four samples are included in Fig. 6. The weight loss takes place in several steps. The first weight loss is due to the removal of interlayer, weakly bonded, water molecules. The second weight loss is attributed to the removal of the interlayer anions (if these undergo thermal decomposition) and water molecules from condensation of the layer hydroxyl groups (36, 37). In some cases, these two processes are recorded as two different, consecutive weight losses (sample 2N) while in other cases a single step is seen (sample 4N). These differences are more evident in the DTA curves (Fig. 6): the endothermic peak corresponding to the second weight loss (removal of hydroxyl groups and nitrate anions) is recorded as a single peak for sample 4N while two peaks are observed for sample 2N.

Similar patterns are recorded for samples 2B and 2Si, although in these cases the weight loss percentage due to the decomposition of the interlayer anions is less significant than in the carbonate or nitrate removal (38). The final weight after calcination at 900°C for nitrate and carbonate containing hydrotalcites amounts ca. 50% of the initial weight. For borate and silicate-containing hydrotalcites the final weight is ca. 65–70% of the initial weight while for vanadate-containing hydrotalcites it is ca. 50–55% of the initial weight (19, 20). Since the PXRD analysis of the residue after calcination indicates the presence of a mixture of oxides the TG weight loss may be used to estimate the amount of interlayer water molecules (Table 1).

The DTA results have been related with the PXRD study of the solids obtained after calcination at increasing temperatures. The PXRD patterns of the calcined samples are included in Figs. 7, 8, and 9. The patterns of sample 2N (Fig. 7) indicate that the layered structure is maintained at temperatures up to 250°C, only a decrease in the interlayer space is observed, probably due to the removal of interlayer water molecules. This water loss is related with the broad endothermic DTA peak centered at 155°C and with shoulders at 208 and 243°C (Fig. 6), probably due to the removal of water molecules held with different strengths in the interlayer space (different strength of the hydrogen bonding). The layered structure collapses during the removal of the hydroxyl groups (350–400°C), occurring together with the removal of the nitrate anions and giving rise to an endothermic effect with minima at 345 and 394°C. When the sample is calcined at 400°C, peaks due to poorly crystalline MgO are observed. Finally, when the sample is calcined at 800°C, weak peaks due to a $MgAl_2O_4$ spinel (4.71, 3.78, 2.844 Å)

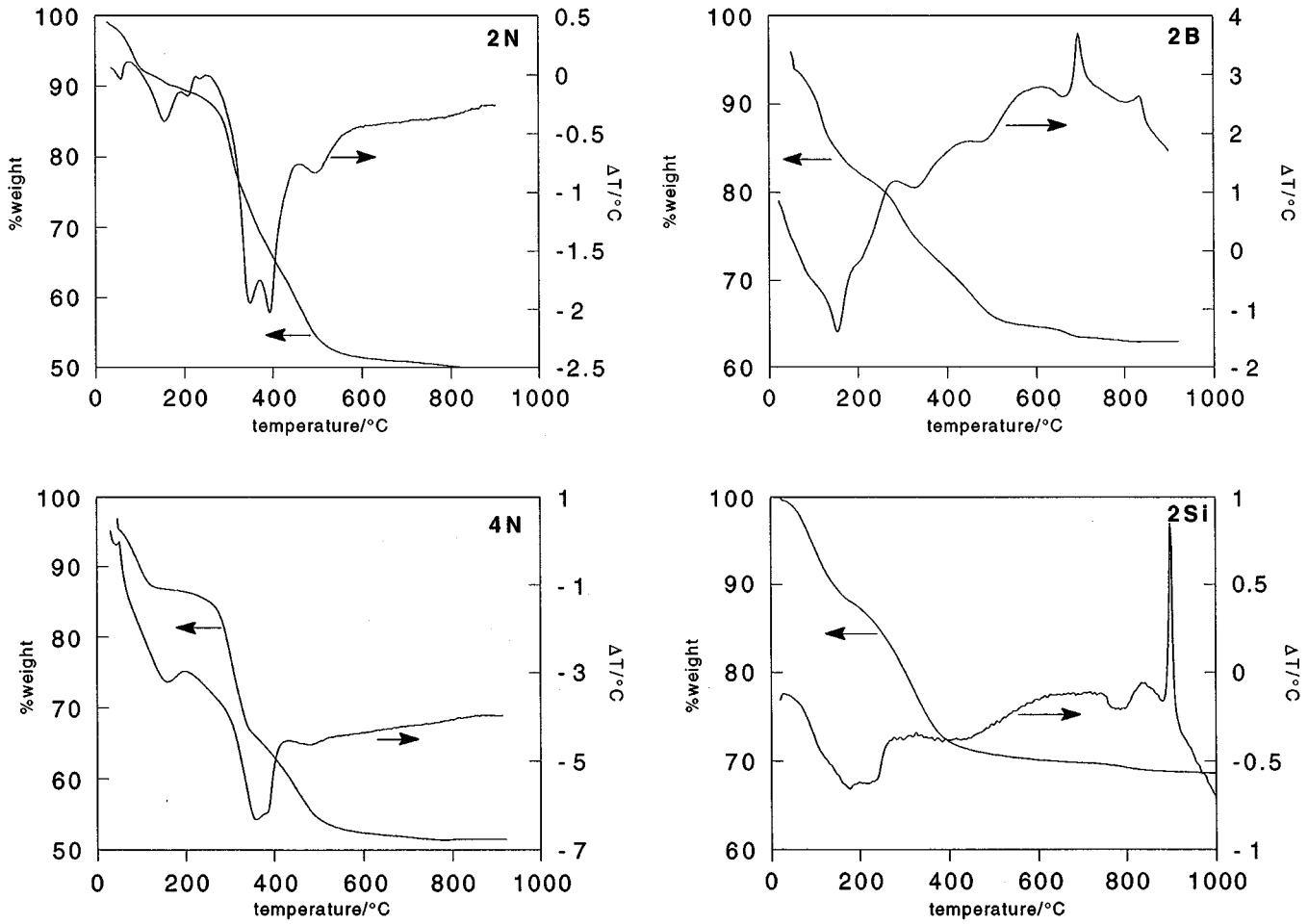

FIG. 6. Thermogravimetric (left axis) and differential thermal (right axis) analysis of precursors 2N and 4N and samples 2B and 2Si.

and to a small amount of Al_2O_3 (7.7 Å) are recorded. Overall, the decomposition follows a pattern similar to that previously reported for similar materials (39–43).

With respect to samples containing borate, it should be noted that the layered structure is preserved at higher calcination temperatures. For sample 2B (Fig. 8), harmonics due to diffraction by (00l) planes are recorded even after calcination at 400°C, although (as observed for the nitrate-containing samples) the interlayer (003) space decreases from 10.8 (parent sample) to 6.7 Å (400°C sample) due to removal of the interlayer water molecules. The removal of layer hydroxyl groups and the decomposition of the interlayer borate species are responsible for the endothermic DTA effects at 205, 330, and 487°C (Fig. 6). Calcination at 500°C leads to a completely amorphous material. The exothermic peak at 700°C (Fig. 6) is due to the crystallization of $Mg_2B_2O_5$ (identified by PXRD, Fig. 8) together with a small amount of Al_2O_3. Calcination at 800°C evidences formation of these species in a crystalline form.

The PXRD patterns recorded after calcination of sample 2Si at increasing temperatures are shown in Fig. 9. Calcination at 100°C leads to a decrease in the intensities of the basal peaks, particularly the planes (003) and (006). This effect is conspicuous upon calcination at 250°C, although some broad and faint PXRD peaks in positions ($2\theta = 22$, 35, and 60) close to those of the hydrotalcite are still observed. We note that the absence of a sharp peak at 4.0 Å definitely discards the possible presence of cristobalite in this sample. An amorphous material giving only a broad PXRD peak between $2\theta = 15$ and 40° is recorded after calcination at 400–700°C. This broad peak is characteristic of mostly amorphous silica, and it seems to coincide with the background diffraction already recorded for the uncalcined sample. Sharp diffraction maxima are recorded only when the sample is calcined at 950°C. In contrast with the results generally obtained for most hydrotalcites (40, 41, 43), no diffraction due to MgO is observed in the range ca. 500–800°C. The reflections recorded can be

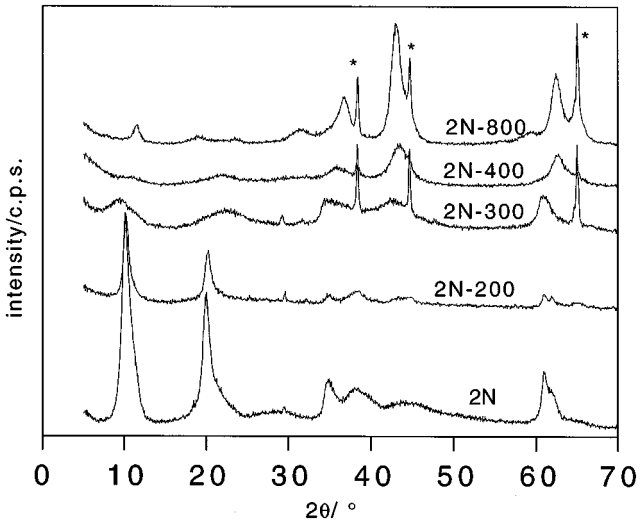

FIG. 7. Powder X-ray diffraction patterns of precursor 2N and matarials calcined at increasing temperatures. The asterisks depict the maxima due to the Al sample holder.

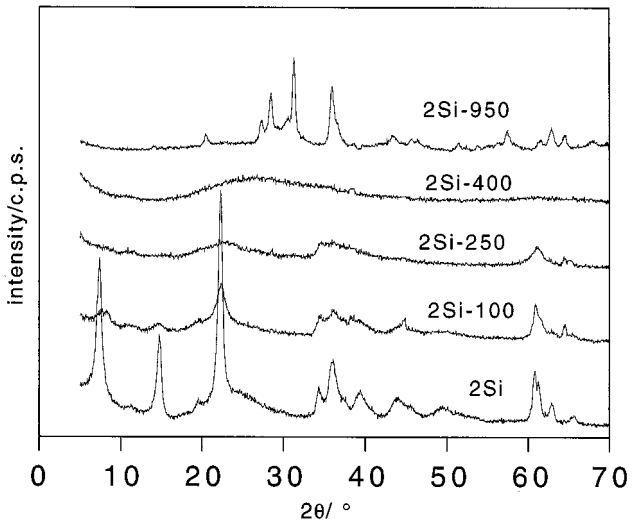

FIG. 9. Powder X-ray diffraction patterns of sample 2Si (original) and materials calcined at increasing temperatures.

ascribed to the formation of clinoenstatite (JCPDS file 35-0610) (30), $MgSiO_3$, the crystallization of which gives rise to the sharp exothermic effect at 900°C. Fyfe *et al.* (15) have previously reported that the calcination of silicate-containing hydrotalcite gives rise to the crystallization of Mg_2SiO_4 when using $[N(Me)_4]_8Si_8O_{20} \cdot xH_2O$ as silicate precursor, and this same species has been also detected by us when using TEOS (tetra ethyl orto silicate) as silicate (44).

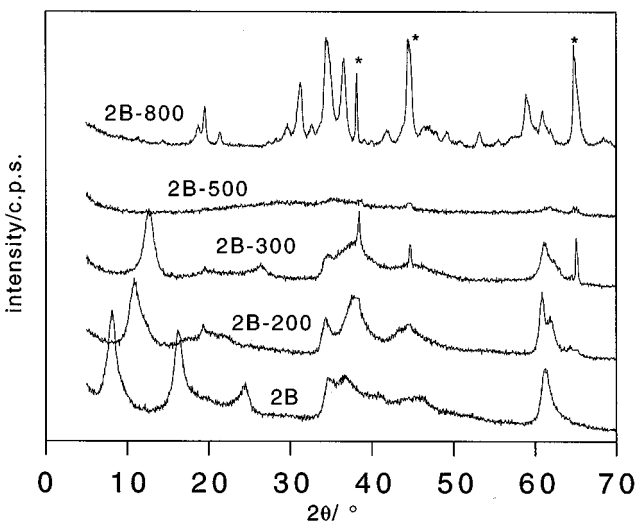

FIG. 8. Powder X-ray diffraction patterns of sample 2B (original) and materials calcined at increasing temperatures. The asterisks depict the maxima due to the Al sample holder.

CONCLUSIONS

Although the interlayer spacing in hydrotalcites strongly depends on the nature of the interlayer anion (this is well known from the literature, and this has been further confirmed in this work with the use of nitrate, borate, and silicate), for "nonspherical" anions the spacing also depends on the precise orientation of the interlayer anion, as suggested for the samples prepared with nitrate. This difference seems to be of paramount importance on the exchange ability of the solid: samples with "tilted" nitrate anions (i.e., larger spacing) exchange incorporating large anions, such as borate and silicate, while those with "flat" oriented nitrate do not exchange. Synthesis under precise pH values avoid depolymerization of tetraborate, which presence in the interlayer space has been undoubtedly concluded from MAS-NMR ^{11}B results. Interlayer tetraborate also enhances the stability of the layered material, in which the structure collpases only after calcination above 500°C, while for nitrate-containing hydrotalcite such a collapse is observed at 350–400°C. On the other hand, *in situ* prepared silicate is incorporated presumably as polymeric $[Si(OSi)_n(O)_{4-n}]^{n-4}$ species with $n = 2$, 3 without the simultaneous presence of any form of silica, which formation has been commonly reported in the literature, nor other LDHs with interlayer carbonate or hydroxyl groups (meixnerite). Upon calcination, an amorphous material is formed between 400 and 700°C, with crystallization of clinoenstatite being observed at 900°C.

ACKNOWLEDGMENTS

Thanks are given to Junta de Castilla y León (Consejería de Educación y Cultura, Grant SA45/98) and Ministerio de Educación y Ciencia (Grants

PB96-1307-C03-01 and IN-96-0252). Support from Portuguese–Spanish Joint Grants Scheme (Ref. HP96-0021 and HP98-0090) is also acknowledged.

REFERENCES

1. F. Trifirò and A. Vaccari, *in* "Comprehensive Supramolecular Chemistry" (J. L. Atwood, J. E. D. Davies, D. D. MacNicol, F. Vogtle, J. M. Lehn, G. Alberti, T. Bein, Eds.), Vol. 7, p. 251. Pergamon–Elsevier Sci. Ltd., Oxford, 1996.
2. F. Cavani, F. Trifiró, and A. Vaccari, *Catal. Today* **11,** 1 (1991).
3. A. de Roy, C. Forano, K. El Malki, and J. P. Besse, *in* "Synthesis of Microporous Materials," Vol. II, Expanded Clays and other Microporous Solids (M. L. Occelli and H. E. Robson, Eds.), p. 108. Van Nostrand Reinhold, New York, 1992.
4. K. Chibwe and W. Jones, *Chem. Mater.* **1,** 489 (1989).
5. T. Kwon, A. Tsigdinos, and T. J. Pinnavaia, *J. Am. Chem. Soc.* **110,** 3653 (1988).
6. M. A. Drezdzon, *Inorg. Chem.* **27,** 4628 (1988).
7. E. D. Dimotakis and T. J. Pinnavaia, *Inorg. Chem.* **29,** 2393 (1990).
8. S. K. Yun and T. J. Pinnavaia, *Inorg. Chem.* **35,** 6853 (1996).
9. M. A. Ulibarri, F. M. Labajos, V. Rives, R. Trujillano, W. Kagunya, and W. Jones, *Inorg. Chem.* **33,** 2592 (1994).
10. V. Rives and M. A. Ulibarri, *Coord. Chem. Rev.* **181,** 61 (1999).
11. S. Cheng and J. T. Lin, *in* "Synthesis of Microporous Materials, Vol. II. Expanded Clays and Other Microporous Solids" (M. L. Occelli and H. E. Robson Eds.), p. 170. Van Nostrand Reinhold, New York, 1992.
12. C. Li, S. Ma, X. Liu, Y. Yue, J. Hui, R. Xu, Y. Bao, and J. Rocha, *Chem. Mater.* **8,** 204 (1996).
13. A. Bhattacharyya and D. B. Hall, *Inorg. Chem.* **31,** 3869 (1992).
14. A. Schutz and P. Biloen, *J. Solid State Chem.* **68** (1987) 360.
15. C. A. Fyfe, G. Fu, and H. Grondey, *Mater. Res. Soc. Symp. Proc.* **346,** 907 (1994).
16. S. K. Yun, V. R. L. Constantino, and T. J. Pinnavaia, *Clays Clay Miner.* **43,** 503 (1995).
17. F. Kooli, V. Rives, and M. A. Ulibarri, *Inorg. Chem.* **34,** 5114 (1995).
18. F. Kooli, V. Rives, and M. A. Ulibarri, *Inorg. Chem.* **34,** 5122 (1995).
19. M. del Arco, M. V. G. Galiano, V. Rives, R. Trujillano, and P. Malet, *Inorg. Chem.* **35,** 6362 (1996).
20. M. del Arco, V. Rives, R. Trujillano, and P. Malet, *J. Mater. Chem.* **6,** 1419 (1996).
21. A. S. Bookin, V. I. Cherkashin, and V. Drits, *Clays Clay Miner.* **41,** 558 (1993).
22. A. S. Bookin and V. Drits, *Clays Clay Miner.* **41,** 551 (1993).
23. P. Gay, "The Crystalline State. An Introduction," 3rd. ed. Oliver and Boyd, Edinburgh, 1972.
24. J. E. Huheey, E. A. Keiter, and R. L. Keiter, "Inorganic Chemistry: Principles of Structure and Reactivity," 4th ed., Harper Collins, New York, 1993.
25. E. C. Kruissink, L. L. Van Reijen, and J. R. H. Ross, *J. Chem. Soc. Faraday Trans I* **77,** 649 (1981).
26. F. M. Labajos, V. Rives, and M. A. Ulibarri, *Spectrosc. Lett.* **24,** 499 (1991).
27. G. Engelhardt and D. Michel, "High-Resolution Solid-State NMR of Silicates and Zeolites," Wiley, New York, 1987.
28. K. F. M. G. J. Scholle and W. S. Veeman, *Zeolites* **5,** 118 (1985).
29. T. Kwon and T. J. Pinnavaia, *Chem. Mater.* **1,** 381 (1989).
30. JCPDS: Joint Committee on Powder Diffraction Standards. International Centre for Diffraction Data, Pennsylvania, 1977.
31. K. Nakamoto, "Infrared and Raman Spectra of Inorganic and Coordination Compounds," 5th. ed. Wiley, New York, 1997.
32. D. L. Bish and G. W. Brindley, *Am. Miner.* **62,** 458 (1977).
33. A. N. Lazarev, *in* "Vibrational Spectra and Structure of Silicates." C/B Consultants Bureau, New York/London, 1972.
34. E. J. J. Groenen, C. A. Emeis, J. P. Van der Berg, and P. C. de Jong-Versloot, *Zeolites* **7,** 474 (1987).
35. S. Gutiérrez, M.Sc. thesis, University of Salamanca, Spain, 1999.
36. L. Pesic, S. Salipurovic, V. Markovic, D. Vucelic, W. Kagunya, and W. Jones, *J. Mater. Chem.* **2,** 1069 (1992).
37. V. Rives, *Inorg. Chem.* **38,** 406 (1999).
38. I. C. Chisem, W. Jones, C. Martín, and V. Rives, *J. Mater. Chem.* **8,** 1917 (1998).
39. T. Sato, K. Kato, T. Endo, and M. Shimada, *React. Solids* **2,** 253 (1986).
40. T. Sato, H. Fujita, T. Endo, and M. Shimada, *React. Solids* **5,** 219 (1988).
41. F. M. Labajos, V. Rives, and M. A. Ulibarri, *J. Mater. Sci.* **27,** 1546 (1992).
42. F. Rey, V. Fornes, and J. M. Rojo, *J. Chem. Soc. Faraday Trans.* **88,** 2233 (1992).
43. J. Rocha, M. del Arco, V. Rives, and M. A. Ulibarri, *J. Mater. Chem.* **9,** 2499 (1999).
44. M. del Arco, C. Martín, J. Rocha, and V. Rives, submitted for publication.